JOURNAL OF SOLID STATE CHEMISTRY 137, 276–282 (1998)
ARTICLE NO. SC977733

Structure and Magnetic Susceptibility of $Mn_{11}Ta_4O_{21}$ and Refinement of the $Mn_4Ta_2O_9$ Structure

J. Grins*,[1] and A. Tyutyunnik†

*Department of Inorganic Chemistry, Arrhenius Laboratory, Stockholm University, S-106 91 Stockholm, Sweden; and †Institute of Solid State Chemistry, Ural Branch of Russian Academy of Sciences, Ekaterinburg GSP-145, 620219 Russia

Received September 3, 1997; accepted December 5, 1997

The structure of $Mn_{11}Ta_4O_{21}$ has been determined and refined using the Rietveld method with combined Cu$K\alpha_1$ X-ray and time-of-flight neutron powder data in space group $P\bar{3}c1$ to $R_{F^2} = 1.3\%$ (neutron data) and $R_{F^2} = 7.8\%$ (X-ray data). The unit cell is $a = 5.3776(2)$ Å, $c = 34.040(2)$ Å, $V = 852.5$ Å^3, and $Z = 2$. The structure consists of a 14-layer hexagonal sequence of close packed oxygen atoms and an ordered distribution of metal atoms in octahedral coordination. It can be described as built up of corundum-type $Mn_4Ta_2O_9$ blocks, with six layers of octahedra, alternating with single MnO layers of octahedra. The structure is compared with that of corundum-related $Mn_4Ta_2O_9$, with unit cell $a = 5.3306(2)$ Å, $c = 14.336(1)$ Å, $V = 352.8$ Å^3, and $Z = 2$, which has been refined in space group $P\bar{3}c1$ to $R_{F^2} = 1.9\%$, using constant-wavelength ($\lambda = 1.47$ Å) neutron powder diffraction data. The magnetic susceptibility of $Mn_{11}Ta_4O_{21}$ exhibits a maximum at 23 K and a Curie–Weiss behavior at higher temperatures with $\Theta_a = -240$ K and $\mu_{eff} = 5.7\ \mu_B$ per Mn atom.

INTRODUCTION

The phase relations of Mn–Ta oxides at low oxygen partial pressures have been studied by Turnock (1), who found that four Mn–Ta oxides were stable at 1200°C and an oxygen pressure of 10^{-17} atm: $MnTa_2O_6$ with an orthorhombic columbite type structure (2), $Mn_4Ta_4O_9$ with a corundum-related structure (3), and two compounds with approximate compositions $Mn_{1.4}TaO_{3.9}$ and $Mn_6Ta_2O_{11}$ and unknown structures. These oxides were prepared by us, in order to be used as precursors for nitridation with ammonia gas, in connection with attempts to synthesize new Mn–Ta (oxy)nitrides (4). The present work shows that the correct composition for the "$Mn_6Ta_2O_{11}$" phase is $Mn_{11}Ta_4O_{21}$; it comprises a determination and refinement of the structure of this compound from X-ray and neutron powder diffraction data and a determination of its magnetic susceptibility.

[1] To whom correspondence should be addressed.

A refinement of the structure of $Mn_4Ta_4O_9$ was also carried out, using neutron powder diffraction data, for comparison with that of $Mn_{11}Ta_4O_{21}$.

EXPERIMENTAL

The $Mn_4Ta_2O_9$ and "$Mn_6Ta_2O_{11}$" compounds were synthesized by heat-treating mixtures of fine-grained Ta_2O_5 and Mn oxalate in an Ar atmosphere, using Ni crucibles and a graphite furnace. The pelleted mixtures were heated to 900°C over 2 h, held there for 12 h, repelleted, and again heat-treated for 12 h at 1200°C. The obtained sintered $Mn_4Ta_2O_9$ pellets were violet, turning pale pink with grinding. The surface layer of the obtained "$Mn_6Ta_2O_{11}$" pellets was violet, containing the oxide $Mn_4Ta_2O_9$, and was therefore removed by polishing. The interior of the pellets was brown and well crystallized, and became pale brown when ground.

XRPD (X-ray powder diffraction) patterns were recorded with a focusing camera of the Guinier–Hägg type, using Cu$K\alpha_1$ radiation and Si as an internal standard. The films were evaluated with a film scanner system (5). XRPD data for Rietveld refinements of $Mn_{11}Ta_4O_{21}$ were collected with a STOE STADI/P diffractometer, using Cu$K\alpha_1$ radiation, a sample in symmetrical transmission mode, and a linear position-sensitive detector covering 4.6° in 2θ. Time-of-flight powder neutron diffraction data of $Mn_{11}Ta_4O_{21}$ were collected on the Polaris diffractometer at the UK spallation neutron source ISIS, Rutherford Appleton Laboratory, and the normalized patterns were corrected for sample absorption effects. Constant-wavelength ($\lambda = 1.47$ Å) neutron powder diffraction data of $Mn_4Ta_2O_9$ were collected at the Swedish research reactor R2 in Studsvik. Data were collected between 10° and 128°. The Rietveld structure refinements were made with the GSAS program package (6), which allows several data sets to be used simultaneously.

A JEOL JSM-820 SEM (scanning electron microscope) with an EDX (energy-dispersive X-ray) microanalysis

0022-4596/98 $25.00

system (LINK AN 10000) was used to determine the metal compositions by averaging 20 EDX point analyses, the statistical error in each being ca. 1 at.%.

Magnetic measurements were carried out in a weak-field ac susceptometer (Lake Shore 7130) in the temperature range 15–330 K, using a magnetic field of 44 A m^{-1} and a frequency of 500 Hz.

RESULTS

Compositional Analysis

SEM EDX analysis of the monophasic $Mn_4Ta_2O_9$ sample yielded a metal content of 66(1) at.% Mn. For "$Mn_6Ta_2O_{11}$" the determined metal content was 72(1) at.% Mn. The analysis showed that the latter material contained a smaller amount of MnO as an impurity. These results suggested that the correct metal composition of "$Mn_6Ta_2O_{11}$" might contain less than the nominal 75 at.% Mn.

Powder Diffraction

The indexed Guinier–Hägg powder pattern of $Mn_4Ta_2O_9$, given in Table 1, yielded the hexagonal unit cell parameters $a = 5.3306(2)$ and $c = 14.336(1)$ Å, in fair agreement with those given in ref 3 ($a = 5.337$ and $c = 14.333$ Å).

The Guinier–Hägg powder pattern of $Mn_{11}Ta_4O_{21}$ ("$Mn_6Ta_2O_{11}$") was first indexed with an hexagonal unit cell, with $a = 5.3776(2)$ and $c = 17.021(2)$ Å, using the program TREOR (7), leaving two reflections unindexed. One of these could be assigned to MnO, while the remaining one, with an intensity of 6% relative to the strongest reflection, remained unaccounted for. It could, however, be indexed as (117) using a unit cell with $a = 5.3776(2)$ Å, $c = 34.040(2)$ Å, and $V = 852.5$ Å^3, i.e., with a doubled c axis. The indexed powder pattern is given in Table 2 for the first 20 observed lines.

The reflections in the neutron powder pattern for $Mn_{11}Ta_4O_{21}$ could all be indexed with the larger cell or assigned to MnO. Systematic reflection absences in the X-ray and neutron powder patterns ($h0l$, $l \neq 2n$) indicated $P3c1$ and $P\bar{3}c1$ as possible trigonal space groups.

The circumstance that all reflections in the X-ray powder pattern except a weak one can be indexed with $c = 17.021(2)$ Å, i.e., with a halved c axis, can be readily explained as follows. The structure determination (see later) shows that the periodicity along the c axis is determined by the oxygen atom positions and that the metal atom arrangement in itself can be described by a unit cell with half of the true c axis. Consequently, only the oxygens contribute to hkl reflections with $l \neq 2n$, and these reflections are weak in the X-ray case since the oxygens contribute only ca. 20% of the total X-ray scattering power. In the neutron case the intensities are different, of course, and the (117) reflection is in fact the strongest one.

TABLE 1
Powder X-Ray Diffraction Pattern of $Mn_4Ta_2O_9$

h	k	l	$2\theta_{obs}$ (deg)	$\Delta 2\theta$ (deg)	d_{obs} (Å)	I/I_0 (%)
0	0	2	12.358	0.020	7.16	2
1	0	0	19.205	− 0.006	4.618	68
1	0	2	22.915	0.020	3.878	20
0	0	4	24.833	0.011	3.583	6
1	0	4	31.564	− 0.014	2.832	100
1	1	0	33.590	− 0.007	2.666	82
1	1	2	35.917	− 0.002	2.4983	2
0	0	6	37.615	− 0.000	2.3894	3
1	1	3	38.651	0.001	2.3277	7
2	0	0	38.989	− 0.001	2.3083	8
2	0	2	41.059	0.011	2.1965	2
1	1	4	42.219	− 0.002	2.1388	10
1	0	6	42.569	− 0.001	2.1220	6
2	0	4	46.783	0.009	1.9403	55
0	0	8	50.912	− 0.004	1.7921	1
1	1	6	51.317	0.005	1.7790	47
2	1	0	52.413	0.017	1.7443	10
2	1	2	54.058	0.010	1.6950	3
1	0	8	54.924	0.008	1.6703	12
2	0	6	55.298	0.006	1.6599	5

Note. $\Delta 2\theta = 2\theta_{obs} - 2\theta_{calc}$. $\lambda = 1.5406$ Å. $a = 5.3306(2)$ Å, $c = 14.336(1)$ Å, $V = 352.8$ Å^3. Cell figure of merit $M_{20} = 122$, $F_{20} = 113(0.00772, 23)$.

TABLE 2
Powder X-Ray Diffraction Pattern of $Mn_{11}Ta_4O_{21}$

h	k	l	$2\theta_{obs}$ (deg)	$\Delta 2\theta$ (deg)	d_{obs} (Å)	I/I_0 (%)
0	0	6	15.605	− 0.002	5.67	4
1	0	0	19.038	− 0.003	4.658	2
1	0	2	19.749	0.001	4.492	44
0	0	8	20.859	− 0.001	4.255	5
1	0	4	21.730	− 0.006	4.087	36
1	0	6	24.704	0.009	3.601	1
0	0	10	26.166	0.009	3.403	1
1	0	10	32.552	− 0.003	2.748	97
1	1	0	33.292	− 0.003	2.689	100
1	1	4	34.967	− 0.001	2.564	2
1	1	6	36.973	0.006	2.4293	6
1	0	12	37.087	0.008	2.4221	7
1	1	7	38.220	0.003	2.3529	6
2	0	2	39.011	0.002	2.3070	5
1	1	8	39.626	0.008	2.2726	8
2	0	4	40.130	0.016	2.2452	3
1	1	10	42.831	0.007	2.1097	3
2	0	8	44.326	0.018	2.0419	1
1	0	16	46.901	− 0.012	1.9356	2
2	0	10	47.273	0.018	1.9213	61

Note. $\Delta 2\theta = 2\theta_{obs} - 2\theta_{calc}$. $\lambda = 1.5406$ Å. $a = 5.3776(2)$ Å, $c = 34.040(2)$ Å, $V = 852.5$ Å^3. Cell figure of merit $M_{20} = 63$, $F_{20} = 83(0.00676, 36)$. Reflection intensities originate from diffractometer data.

Refinement of the Structure of $Mn_4Ta_2O_9$

The corresponding coordinates for $Mn_4Nb_2O_9$ (3) were used as starting values. The theoretical number of reflections for $2\theta < 128^\circ$ was 243, and the half-width of the peaks was 0.30° at $2\theta = 50^\circ$. A total of 43 parameters were refined: 7 positional and 5 isotropic thermal parameters for $Mn_4Ta_2O_9$, 20 coefficients for the Chebyshev background polynomial, 7 profile parameters for the pseudo-Voigt function (8) used, 2 lattice parameters and the zero point, and the scale factor. The agreement of the calculated and observed diffraction patterns is shown in Fig. 1. The corresponding refinement indices are $R_{wp} = 0.046$, $R_p = 0.036$, and $R_{F^2} = 0.019$, *Dwd* (Durbin–Watson *D* value) = 1.57, and $S = 1.17$. The obtained atomic coordinates are given in Table 3, and selected interatomic distances in Table 4. The use of anisotropic thermal parameters yielded no substantial improvements.

Determination and Refinement of the Structure of $Mn_{11}Ta_4O_{21}$

The structure was solved from the following considerations: (i) The length of the *c* axis suggests that there are 14 hexagonal layers of close-packed oxygens, with three oxygens per layer and a total of 42 oxygens in the unit cell. (ii) The metal atoms were assumed to be in special positions at $(0, 0, z)$, $(\frac{1}{3}, \frac{2}{3}, z)$ or $(\frac{2}{3}, \frac{1}{3}, z)$, i.e, situated in rows parallel to the *c* axis. (iii) The number of metals in these three types of columns were assumed to be equal. (iv) The initial nominal composition of the compound is $Mn_6Ta_2O_{11}$ (75 at.% Mn), or $Mn_{24}Ta_8O_{44}$. The compositional analysis indicated, however, that the true Mn content might be lower. A conceivable composition, which complies with point i, is $Mn_{22}Ta_8O_{42}$ (73.3 at.% Mn), or $2Mn_{11}Ta_4O_{21}$. If the composition $Mn_{11}Ta_4O_{21}$ is correct, then some of the metal atom layers in the unit cell contain three metal atoms, and these are probably Mn. (v) Vacant octahedral positions are probably not adjacent to each other along the *c* axis. (vi) The centrosymmetric space group $P\bar{3}c1$ was primarily assumed, implying that there are two identical metal arrangements in the unit cell, which are symmetry-related by a translation of $z = \frac{1}{2}$.

Initial Rietveld refinements supported several of these assumptions, in particular point i. The correct metal distribution, however, could not be derived from sets of trial distributions, even by careful refinement of metal site occupancy factors, despite the simultaneous use of the X-ray and neutron data sets. However, a closer examination of possible structures revealed only one arrangement of metal-filled octahedra that is compatible with all the points i–vi. This hypothesis was tested and proved to be correct. The distribution of Mn and Ta atoms over these metal sites was then arrived at by an exhaustive search of possibilities.

The structure was refined using both the X-ray ($2\theta = 10$–120°, with 448 theoretical reflections) and neutron data ($d = 0.5$–3.1 Å, with 2561 theoretical reflections). Converging refinements were achieved when structural and profile fitting parameters were refined in succession. The backgrounds were fitted by 20 Chebyshev polynomial coefficients. The X-ray reflection profiles were modeled by a pseudo-Voigt function (8) with 7 coefficients and the neutron profiles with the function described in ref 9, using 8 coefficients. A Debye–Scherrer absorption coefficient was refined for the X-ray data. The *d* and 2θ scales for the

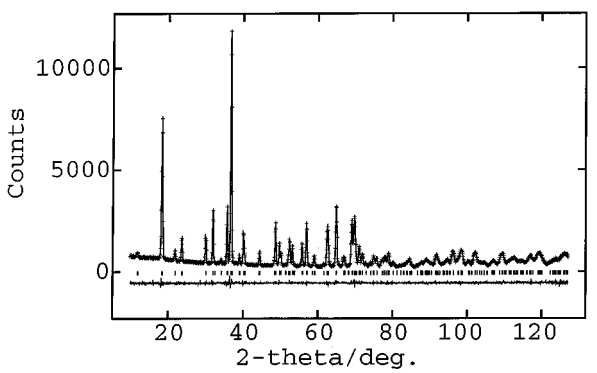

FIG. 1. Observed (crosses), calculated (solid line), and difference (bottom) neutron diffraction patterns of $Mn_4Ta_2O_9$.

TABLE 3
Structural Parameters Refined from Neutron Powder Diffraction Data for $Mn_4Ta_2O_9$

Atom	Site	*x*	*y*	*z*	U_{eq} (Å^2)
Mn1	4*d*	$\frac{1}{3}$	$\frac{2}{3}$	0.0192(2)	0.0070(10)
Mn2	4*d*	$\frac{1}{3}$	$\frac{2}{3}$	0.3040(2)	0.0066(10)
Ta	4*c*	0	0	0.3565(1)	0.0034(5)
O1	6*f*	0.2770(4)	0	1/4	0.0056(6)
O2	12*g*	0.3349(3)	0.3068(3)	0.0862(1)	0.0071(4)

Note. Trigonal, $a = 5.3306(2)$ Å, $c = 14.336(1)$ Å, $V = 352.8$ Å^3, $Z = 2$, $P\bar{3}c1$.

TABLE 4
Atomic Distances (Å) in $Mn_4Ta_2O_9$

Mn1–O2 × 3	2.147(2)	Mn2–O1 × 3	2.093(2)
–O2 × 3	2.281(3)	–O2 × 3	2.322(3)
Mean	2.214	Mean	2.208
Ta–O2 × 3	1.899(2)	Ta–Ta	3.053(4)
–O1 × 3	2.124(2)	Mn1–Mn2	3.086(5)
Mean	2.012		

TABLE 5
Structural Parameters Refined from X-Ray and Neutron Powder Diffraction Data for $Mn_{11}Ta_4O_{21}$

Atom	Site	x	y	z	U_{eq} (Å^2)
Mn1	4*c*	0	0	0.08803(8)	0.0058
Mn2	4*d*	$\frac{1}{3}$	$\frac{2}{3}$	0.97992(11)	0.0165
Mn3	4*d*	$\frac{1}{3}$	$\frac{2}{3}$	0.15707(12)	0.0187
Mn4	4*d*	$\frac{2}{3}$	$\frac{1}{3}$	0.13486(12)	0.0120
Mn5	4*d*	$\frac{2}{3}$	$\frac{1}{3}$	0.22668(11)	0.0080
Mn6	2*b*	0	0	0	0.0082
Ta1	4*d*	$\frac{1}{3}$	$\frac{2}{3}$	0.07025(7)	0.0075
Ta2	4*c*	0	0	0.20536(5)	0.0067
O1	12*g*	0.6530(4)	0.6999(4)	0.03703(5)	0.0125
O2	12*g*	0.3460(4)	0.3814(3)	0.10637(5)	0.0085
O3	12*g*	0.6985(4)	0.6684(3)	0.18104(5)	0.0089
O4	6*f*	0.2752(3)	0.2752(3)	$\frac{1}{4}$	0.0081

Note. Trigonal, $a = 5.3776(2)$ Å, $c = 34.040(2)$ Å, $V = 852.5$ Å^3, $Z = 2$, $P\bar{3}c1$.

TABLE 7
Atomic Distances (Å) in $Mn_{11}Ta_4O_{21}$

Mn1–O2 × 3	2.060(2)	Mn2–O1 × 3	2.090(2)
–O1 × 3	2.468(3)	–O1 × 3	2.541(3)
Mean	2.264	Mean	2.316
Mn3–O3 × 3	2.122(2)	Mn4–O2 × 3	2.104(3)
–O2 × 3	2.332(3)	–O3 × 3	2.332(3)
Mean	2.227	Mean	2.218
Mn5–O4 × 3	2.122(2)	Mn6–O1 × 6	2.160(2)
–O3 × 3	2.320(3)		
Mean	2.221		
Ta1–O1 × 3	1.990(2)	Ta2–O3 × 3	1.898(2)
–O2 × 3	1.993(2)	–O4 × 3	2.121(2)
Mean	1.992	Mean	2.010
Ta2–Ta2	3.039(3)	Mn4–Mn5	3.126(6)
Ta–Mn2	3.075(4)	Mn1–Mn6 × 2	2.997(3)
–Mn3	2.955(5)		

neutron and X-ray data were mutually adjusted by successive refinements of these and the cell parameters. MnO was included as a second phase with two thermal parameters, the lattice parameter and and the phase fraction refined. Seventeen positional parameters and 46 anisotropic thermal parameters were refined for $Mn_{11}Ta_4O_{21}$. The use of anisotropic thermal parameters significantly improved the fit to the neutron data. The obtained atomic coordinates are given in Table 5, the thermal parameters in Table 6, and selected interatomic distances in Table 7. The fit between observed and calculated patterns for the X-ray and neutron data is illustrated in Figs. 2 and 3, respectively. The corresponding refinement indices are $R_{wp} = 0.020$, $R_p = 0.015$, $Dwd = 0.68$, and $R_{F^2} = 0.013$ for the neutron data and $R_{wp} = 0.016$, $R_p = 0.031$, $Dwd = 1.098$, and $R_{F^2} = 0.078$ for the X-ray data, with a total χ^2 of 1.11. The refined phase fraction of MnO was 2.1 wt%, corresponding to a total metal Mn content of 74.2 at.%, to be compared with the nominal value of 75 at.%.

TABLE 6
Anisotropic Thermal Parameters (Å$^2 \times 100$) for $Mn_{11}Ta_4O_{21}$

Atom	U_{11}	U_{22}	U_{33}	U_{12}	U_{13}	U_{23}
Mn1	0.61(6)	0.61(6)	0.5(1)	0.31(3)	0	0
Mn2	0.94(8)	0.94(8)	3.1(2)	0.47(4)	0	0
Mn3	1.1(1)	1.1(1)	3.4(3)	0.54(6)	0	0
Mn4	0.7(1)	0.7(1)	2.2(2)	0.35(5)	0	0
Mn5	0.8(1)	0.8(1)	0.8(1)	0.40(4)	0	0
Mn6	1.1(1)	1.1(1)	0.2(2)	0.55(7)	0	0
Ta1	0.67(3)	0.67(3)	0.9(1)	0.34(2)	0	0
Ta2	0.27(4)	0.27(4)	1.4(1)	0.14(2)	0	0
O1	1.31 (7)	0.90(6)	1.71(7)	0.58(5)	0.59(6)	0.35(5)
O2	0.63(5)	0.63(6)	1.30(5)	0.34(4)	− 0.13(5)	0.36(5)
O3	0.92(6)	0.85(5)	0.82(4)	0.37(4)	− 0.28(4)	− 0.23(5)
O4	0.78(5)	0.78(5)	0.65(7)	0.22(5)	0.14(4)	− 0.14(4)

Note. Defined by $T = \exp[-2\pi^2(h^2a^{*2}U_{11} + \cdots + 2hka^*b^*U_{12} + \cdots)]$.

Description of the Stuctures of $Mn_4Ta_2O_9$ and $Mn_{11}Ta_4O_{21}$

The structures of $Ma_4Ta_2O_9$ and $Mn_{11}Ta_4O_{21}$ are illustrated in Fig. 4. The structure of $Mn_4Ta_2O_9$ (3) derives from the corundum type by an ordering of Mn and Ta atoms in a six-layer sequence of hexagonally close-packed oxygen atoms. It contains pairs of face-sharing Mn–O and Ta–O octahedra, with Mn–Mn and Ta–Ta distance of 3.086(5) and 3.053(4) Å, respectively. Because the octahedra share faces, the metal atoms are notably displaced from their centers. The Mn–O distances range from 2.093(3) to 2.322(3) Å and the Ta–O distance from 1.899(2) to 2.124(2) Å. The average Mn–O and Ta–O distances, 2.21

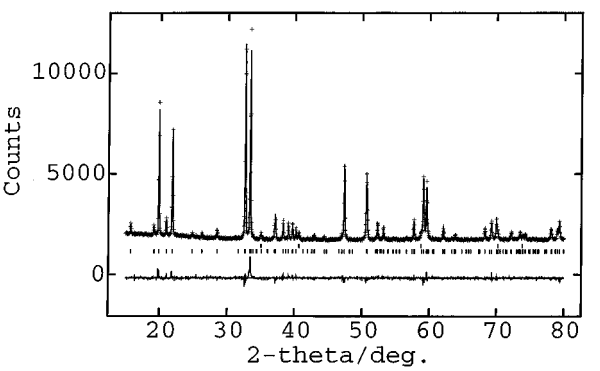

FIG. 2. Observed (crosses), calculated (solid line), and difference (bottom) XRPD patterns of $Mn_{11}Ta_4O_{21}$ for $2\theta = 15$–80°.

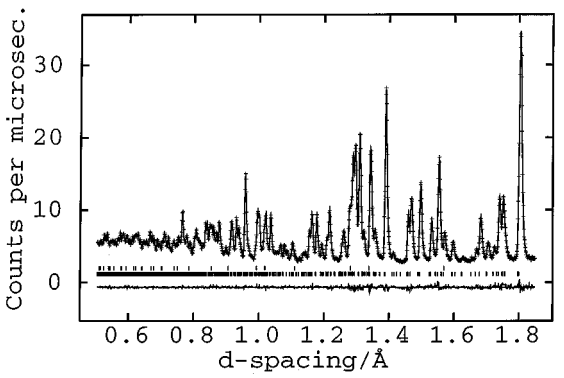

FIG. 3. Observed (crosses), calculated (solid line), and difference (bottom) time-of-flight neutron diffraction patterns of $Mn_{11}Ta_4O_{21}$ for $d = 0.5$–1.85 Å.

and 2.01 Å, respectively, agree well with the expected values of 2.21 and 2.02 Å, calculated from Shannon–Prewitt ionic radii (10) of 0.83, 0.64, and 1.38 Å for Mn^{2+}(HS), Ta^{5+}, and O^{2-} (IV), respectively. Compounds isostructural with $Mn_4Ta_2O_9$ include $M_4Ta_2O_9$ and $M_4Nb_2O_9$, with $M =$ Mg, Co and Fe (3, 11, 12).

The structure of $Mn_{11}Ta_4O_{21}$ exhibits an ordered arrangement of Mn and Ta atoms in a 14-layer sequence of hexagonally close-packed oxygen atoms. The unit cell contains two six-layer corundum type blocks, similar to the ones in $Mn_4Ta_2O_9$ and with compositions $2Mn_4Ta_2O_9$. The metal ordering in these, however, is different from that in $Mn_4Ta_2O_9$. The blocks are interleaved by single layers of octahedra with composition 3MnO at $z = 0$ and $\frac{1}{2}$. The 14-layer sequence may thus be described as

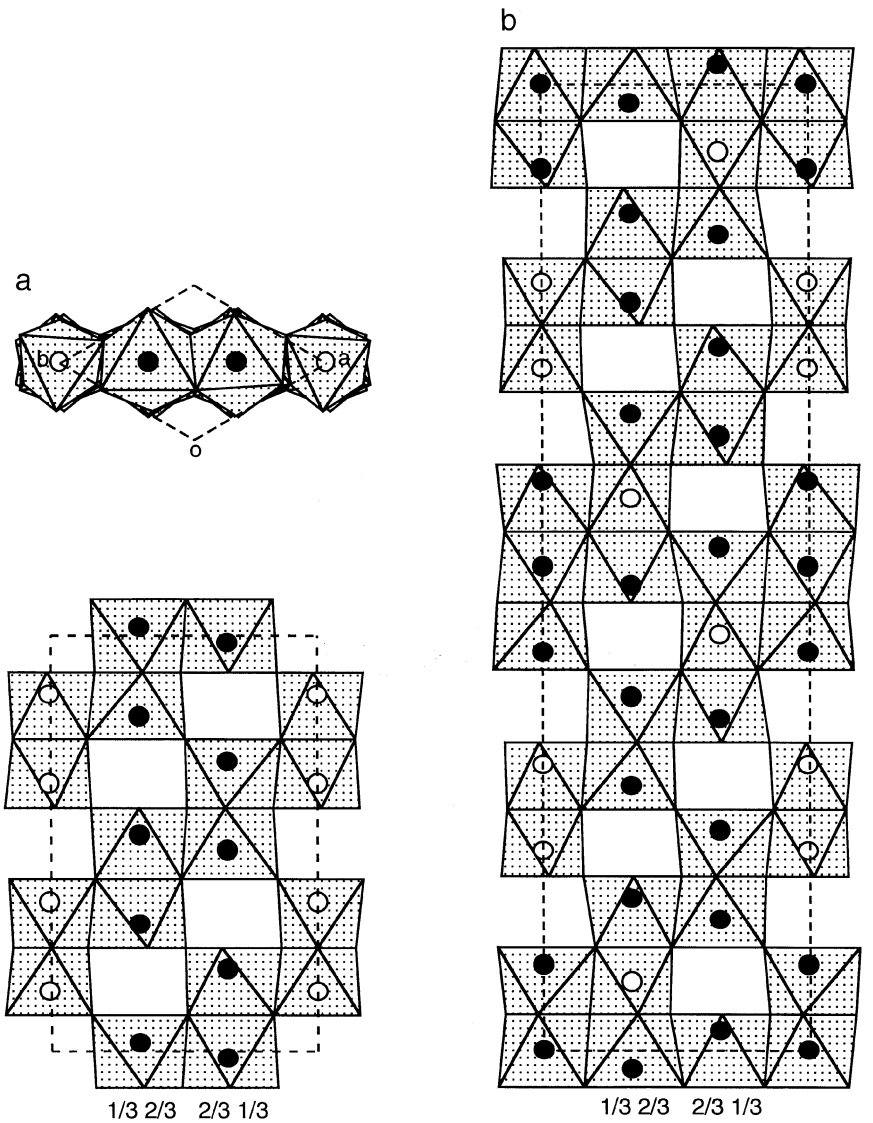

FIG. 4. Illustration of (110) sections in the structures of (a) $Mn_4Ta_2O_9$ and (b) $Mn_{11}Ta_4O_{21}$. The section for $Mn_4Ta_2O_9$ is shown in (a) in a projection on (001). The numbers at the bottom designate the x and y coordinates of the metal atoms. Mn and Ta atom positions are designated by filled and unfilled circles, respectively.

TABLE 8
Bond Valence Sums for $Mn_4Ta_2O_9$ and $Mn_{11}Ta_4O_{21}$

		$Mn_4Ta_2O_9$			
Ta	4.88	Mn1	1.94	O1	2.03
		Mn2	2.04	O2	1.94
		$Mn_{11}Ta_4O_{21}$			
Ta1	4.95	Mn1	1.93	O1	1.94
Ta2	4.93	Mn2	1.73	O2	1.96
		Mn3	1.92	O3	1.94
		Mn4	1.98	O4	1.98
		Mn5	1.94		
		Mn6	2.21		

Note. $v = \exp((R - d)/0.37)$, $R(\text{Ta}) = 1.92$, $R(\text{Mn}) = 1.79$, $R(\text{O}) = 1.48$.

$3MnO–2Mn_4Ta_2O_9–3MnO–2Mn_4Ta_2O_9$. The two corundum type blocks in the unit cell are symmetry-related by a threefold inversion axis. In addition to pairs of face-sharing Mn–O and Ta–O octahedra, the structure also contains triplets of octahedra sharing faces along the *c* axis, some containing solely Mn atoms, with Mn–Mn distances 2.996(3) Å, and some containing 2 Mn atoms and 1 Ta atom, with Ta–Mn distances 2.954(5) and 3.074(4) Å. The Mn—Mn and Ta–Ta distances in the pairs of face-sharing octahedra, 3.125(6) and 3.038(3) Å, respectively, are similar to the corresponding distances found in the structure of $Mn_4Ta_2O_9$. The metal atoms are displaced from the centers of the octahedra, just as in the $Mn_4Ta_2O_9$ structure. The Mn–O distances range from 2.059(2) to 2.541(3) Å and the Ta–O distances from 1.898(2) to 2.121(2) Å. The average Mn–O and Ta–O distances are 2.23 and 2.00 Å, respectively.

Empirical bond valence sums (13) for $Mn_4Ta_2O_9$ and $Mn_{11}Ta_4O_{21}$, calculated from the structural data, are given in Table 8. They are very satisfactory for $Mn_4Ta_2O_9$. In the case of $Mn_{11}Ta_4O_{21}$, though, the bond valence sum for Mn2 is rather low, 1.73, and for Mn6 rather high, 2.21. This may indicate that the refined position of the O1 atom is not completely correct (cf. Table 7).

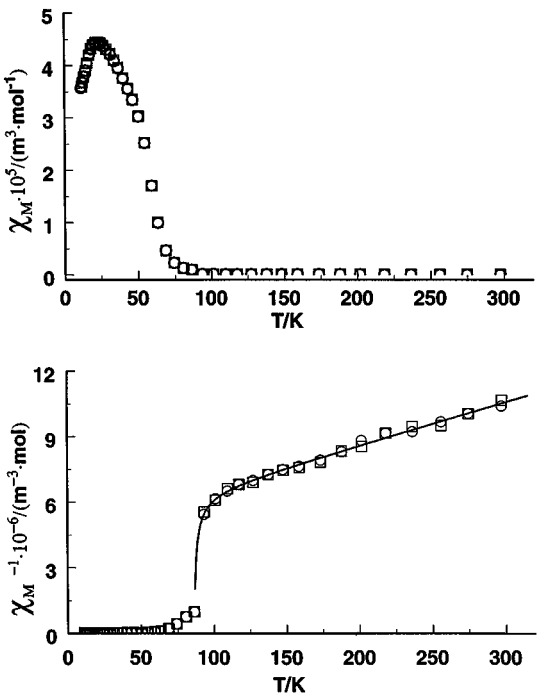

FIG. 5. Molar magnetic susceptibility per Mn atom and its inverse versus temperature for $Mn_{11}Ta_4O_{21}$.

Magnetic Ssusceptibility of $Mn_{11}Ta_4O_{21}$

The magnetic susceptibility per Mn atom, χ_M, of $Mn_{11}Ta_4O_{21}$ and its inverse, χ_M^{-1}, are shown in Fig. 5 as a function of temperature, *T*. A Curie–Weiss law behavior $\chi_M = C/(T - \Theta_a)$ is observed above ca. 100 K and the susceptibility shows a well-defined maximum at 23 K. A fit of the data to the Néel equation for a two-sublattice ferrimagnet, $\chi_M^{-1} = (1/C)[T - \Theta_a - \Theta_b^2/(T - \Theta)]$, yielded the following values of the constants: $C = 5.1(1) \times 10^{-5}\,\text{m}^3\,\text{K}\,\text{mol}^{-1}$, $\Theta_a = -240(11)\,\text{K}$, $\Theta_b^2 = 497(75)\,\text{K}^2$, and $\Theta = 84.8(2)\,\text{K}$. From the Curie constant the effective number of Bohr magnetons per Mn atom (μ_{eff}) was determined to be 5.7(1) μ_B, which agrees with an expected value of 5.9 μ_B for Mn^{2+} in a high-spin state. The small amount of MnO in the sample, 2.1 wt% according to the Rietveld refinement, is estimated to effect an underestimation of the susceptibility of $Mn_{11}Ta_4O_{21}$ in the high-temperature paramagnetic region, and thus also of the μ_{eff} value, of ca. 2%.

CONCLUDING REMARKS

Attempts to synthesize compounds isostructural with $Mn_{11}Ta_4O_{21}$ and with Mg, Ni, Co, Fe, or Zn replacing Mn, were not successful, in agreement with previous findings. The structure type thus appears to be adopted only with the metal combination Mn–Ta.

We have recently collected neutron powder diffraction data of $Mn_{11}Ta_4O_{21}$ at 10 K that show that the magnetic moments of the Mn^{2+} ions are ordered at this temperature. All the Bragg peaks in the low-temperature diffraction pattern can be indexed with the same type of unit cell as the room-temperature data. A substantial number of Bragg peaks, of magnetic origin, are, however, present that do not conform with the systematic absences of the space group $P\bar{3}c1$ ($h0l, l \neq 2n$). An elucidation of the magnetic structure of $Mn_{11}Ta_4O_{21}$ is currently in progress.

ACKNOWLEDGMENTS

The authors thank Dr. S. Eriksson for collecting the TOF neutron data, Dr. A. Tellgren (Studsvik) for providing the facilities for the neutron diffraction work, Mr. H. Rundlöf (Studsvik) for assistance with the collection of neutron diffraction data, and Prof. M. Nygren for support and valuable discussions.

REFERENCES

1. A. C. Turnock, *J. Am. Ceram. Soc.* **49,** 382 (1966).
2. H. Weitzel, *Z. Kristallogr.* **144,** 238 (1976).
3. F. Bertaut, L. Corliss, F. Forrat, R. Aleonard, and R. Pauthenet, *Phys. Chem. Solids* **21,** 234 (1961).
4. J. Grins, P.-O. Käll, and G. Svensson, *J. Solid State Chem.* **117,** 48 (1995).
5. K. E. Johansson, T. Palm, and P.-E. Werner, *J. Phys. E* **13,** 1289 (1980).
6. A. C. Larson and R. B. Von Dreele, Los Alamos National Laboratory Report No. LA-UR-86-748, 1987.
7. P.-E. Werner, L. Eriksson, and M. Westdahl, *J. Appl. Crystallogr.* **18,** 367 (1985).
8. P. Thompson, D. E. Cox, and J. B. Hastings, *J. Appl. Crystallogr.* **20,** 79 (1987).
9. R. B. Von Dreele, J. D. Jorgensen, and C.G. Windsor, *J. Appl. Crystallogr.* **15,** 581 (1982).
10. R. D. Shannon, *Acta Crystallogr., Sect. A* **32,** 751 (1976).
11. A. C. Turnock, *J. Am. Ceram. Soc.* **48,** 258 (1965).
12. G. Halle and Hk. Müller-Buschbaum, *Z. Anorg. Allg. Chem.* **562,** 87 (1988).
13. I. D. Brown and D. Altermatt, *Acta Crystallogr., Sect. B* **41,** 244 (1985).